Substoichiometric ultrathin zirconia films cause strong metal-support interaction

Supplementary Information

Peter Lackner, Joong-Il Jake Choi‡, Ulrike Diebold, and Michael Schmid

Institute of Applied Physics, TU Wien, 1040 Vienna, Austria.

‡ *Present address: Center for Nanomaterials and Chemical Reactions, Institute for Basic Science (IBS) Daejeon 305-701, South Korea.*

1 Variations in the Moiré Structure on Rh(111)

The zigzag moiré pattern of ultrathin zirconia films on Rh(111) can be regular over long distances as in Figures S1a, or less prominent as in Figure S1b and c. The degree of long-range order correlates with the annealing temperature, annealing time, and the amount of deposited material. When the annealing temperature and/or time reaches the values necessary for a full coverage of the ultrathin film, the order of the zigzag moiré pattern decreases with further annealing. For a fully closed film, a moiré pattern that was ordered over large distances was never encountered — closing a film requires higher temperatures if less material is available.

The STM images of Figures S1a and b show two regions of the same experiment (1.2 ML zirconia, $T_{\mathrm{anneal}} = 950\,^{\circ}\mathrm{C}$ in UHV), yet the first image was taken close to the edge of the crystal, where slightly less material was deposited. Therefore, the same T is sufficient in the middle of the crystal for a fully closed film with thin stripes of the zigzag structure, interrupted by stripes not showing the moiré. Few, elongated zigzag patterns reach from one moiré stripe to the next, with no zigzag patterns in between; an example of an elongated zigzag pattern is marked in orange in the bottom image of Figure S1b. After annealing for another 10 min at 950 °C, parts of the film show no zigzag pattern at all, see left half of the bottom image in Figure S1c. In the overview image (top), only small patches of ordered zigzag patterns can be found. The films investigated by XPS (main paper section 3.3, Figure 4) showed a similar pattern. Even when comparing areas with and without any zigzag structure, i.e. the left and right half of the detailed image in Figure S1c, the 0.35 nm zirconia lattice parameter varies by $< 1\%$. This indicates that the differences of the zirconia lattice leading to the different appearance of the moiré are very small, which is not unexpected, since a moiré pattern is very sensitive to small variations of the lattices forming the moiré. To some degree, these small variations may be related to somewhat different stoichiometries of the zirconia film, possibly related to different preparations (stronger reduction at higher temperatures). Unfortunately, we could not determine the lattice parameter of the zirconia lattice with high precision from the morié pattern, because the Rh spots cannot be clearly identified in the FFT which would be required to explain such a complex moiré pattern. As expected from the low amount of Zr dissolved in the Rh substrate, no Fourier spots of an ordered Rh-Zr alloy were found.

2 Uncertainties in XPS-based Stoichiometry Estimation

For the determination of the stoichiometry of the ultrathin zirconia film from the ratio of Zr 3d to O1s XPS peak areas, a standard sample with known composition has to be used. This is due to the unknown transmission function (sensitivity *vs.* electron energy) of the electron analyzer. Bulk zirconia cannot be used as a reference due to its insulating nature (charging), and possibly undetected hydroxylation, which would affect the O:Zr ratio. Although available as single crystal, the same problems affect YSZ, where yttria segregation[1] may come as a further complication. This leaves the possibility of using a well-characterized 5 ML-thick zirconia film as a reference. Even then, problems remain. First and foremost, a 1 ML-thick films cannot be compared directly with thicker films due to energy-dependent attenuation of photoelectrons. To account for this problem, we have simulated the XPS spectra of both systems using the SESSA code.[2] Secondly, the fraction of the surface covered by ultrathin zirconia (excluding the 3D islands) can only be determined locally using STM; this value might vary from position to position (e.g., at step bunches, which are difficult to measure by STM). The problem of unknown area fractions is especially troublesome because we can only determine the combined O 1s signal of the 3D ZrO_2 islands and the ultrathin film (A clear separation of these signals is difficult in synchrotron-based XPS[3] and impossible with a non-monochromated source, see Fig. 4d of the main article). Thirdly, the ZrO_2 film used as standard is not perfectly stoichiometric. This problem is fortunately a minor one, since even slightly-reduced tetragonal and fully-oxidized monoclinic films show the same O:Zr ratio within the error bars,[4] so the tetragonal films used here do not significantly deviate from ZrO_2. Finally, photoelectron diffraction (mainly forward focussing[5]) may be different between ultrathin zirconia and ZrO_2 islands; this is not taken into account by the SESSA simulation. To estimate the extent of forward focussing effects on the O:Zr ratio, XPS was measured under varying emission angle (0°, 15°, 35°, 55° off-normal). The lowest O:Zr ratio was measured for 15° (the standard angle); the other angles led to a maximum increase of $\Delta(\mathrm{O{:}Zr}) = 0.18$. Finally, the accuracy of the method suffers from the unknown amount of O dissolved in the Rh substrate. All these possible errors were estimated and included in the error bars given in the main text.

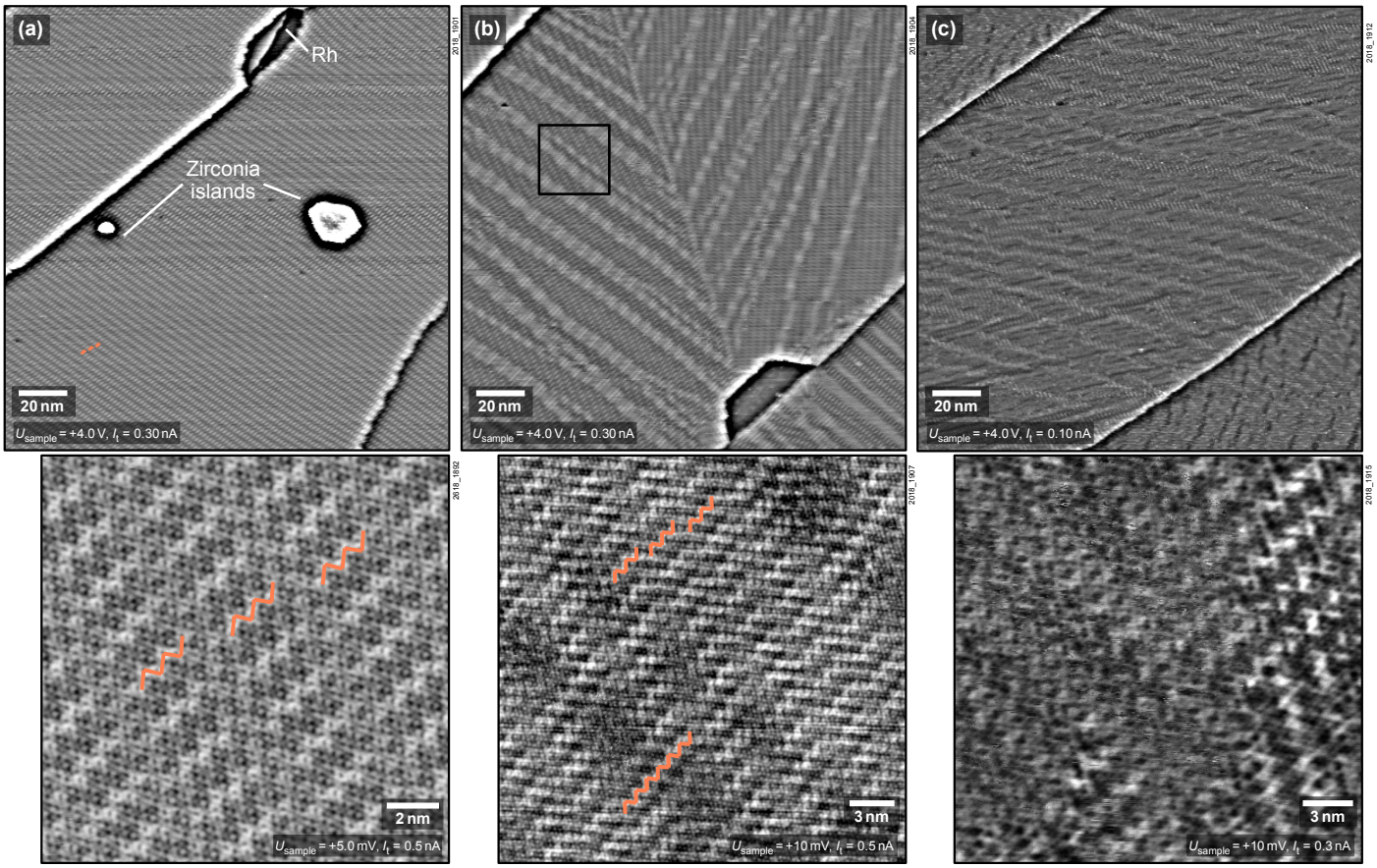

Fig. S1 STM images of ultrathin zirconia films on Rh(111) in different states of ordering. The bottom panels show the structures at higher magnification. **(a)** When the film is not fully closed, the film exhibits large domains with an ordered zigzag moiré structure (orange). **(b)** Fully closed films exhibit zigzag domains only in long stripes (imaged dark in the overview image, bright in the inset, due to different tunneling bias). **(c)** At higher T, the film shows large areas without a zigzag moiré. The overview images at the top are high-pass filtered.

3 Diffusion of Alloyed Zr in Rh and Pt

The diffusion of alloyed Zr was investigated by XPS for Rh(111) and Pt(111), see Figure S2. 0.48 ML of metallic Zr were depositing on each of the two substrates. The samples were annealed in UHV in steps of 110 °C for 10 min each. Due to the high reactivity of Zr, part of the deposited Zr was found in oxidized form (possibly due to adsorption of residual-gas species or oxygen in the sputter target remaining from previous experiments with deposition in mixed O_2–Ar gas), but this signal disappeared after annealing to 640 °C on Rh and 420 °C on Pt. On Pt(111), Zr disappears into the bulk at much lower temperatures than on Rh(111), indicating that the diffusion of Zr is faster in Pt than in Rh. Zr dissolution happens at a lower temperature in Pt due to the more negative dissolution enthalpy (−4.4 to −4.9 eV *vs.* −3.3 eV for Zr in Pt and Rh, respectively[6,7]). Also, the formation energy of Pt_3Zr (−128 kJ/g-atom[8], an Engel-Brewer alloy[9]) is lower than for Rh_3Zr (−72 kJ/g-atom.[10]) The lattice constant of Rh is smaller than for Pt (0.2687 nm *vs.* 0.2775 nm, respectively), which makes dissolution of the large Zr atoms less favorable. Furthermore, Rh has a higher melting point than Pt (1964 °C *vs.* 1768 °C, respectively). Thus, diffusion in Rh tends to be slower than in Pt.

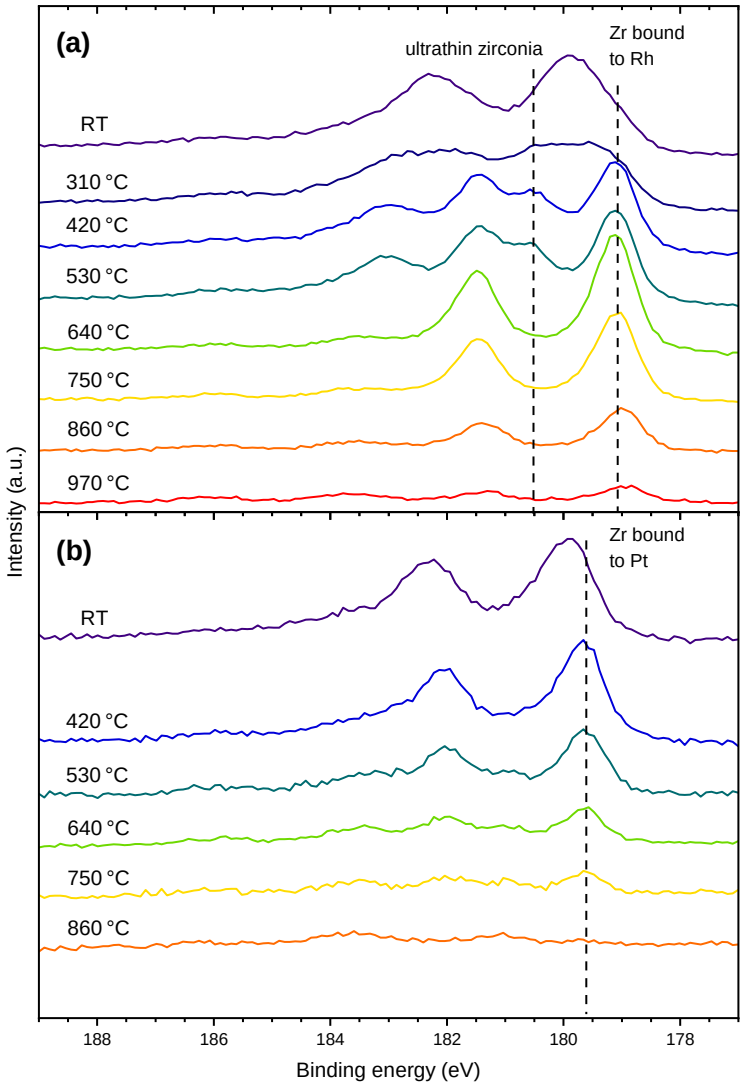

Fig. S2 XPS of diffusion of 0.48 ML Zr into **(a)** Rh(111) and **(b)** Pt(111). After deposition, small amounts of oxidized Zr are present, but vanish soon. Metallic Zr disappears faster into the Pt bulk compared with Rh. All spectra are normalized to the background on the low-binding-energy side.

References

1 D. Majumdar and D. Chatterjee, X-ray photoelectron spectroscopic studies on yttria, zirconia, and yttria-stabilized zirconia, *J. Appl. Phys.*, 1991, **70**, 988–992, DOI: 10.1063/1.349611.

2 W. Smekal, W. S. M. Werner and C. J. Powell, Simulation of electron spectra for surface analysis (SESSA): a novel software tool for quantitative Auger-electron spectroscopy and X-ray photoelectron spectroscopy, *Surf. Interface Anal.*, 2005, **37**, 1059–1067, DOI: 10.1002/sia.2097.

3 H. Li, J.-I. J. Choi, W. Mayr-Schmölzer, C. Weilach, C. Rameshan, F. Mittendorfer, J. Redinger, M. Schmid and G. Rupprechter, Growth of an ultrathin zirconia film on Pt_3Zr examined by high-resolution X-ray photoelectron spectroscopy, temperature-programmed desorption, scanning tunneling microscopy, and density functional theory, *J. Phys. Chem. C*, 2015, **119**, 2462–2470, DOI: 10.1021/jp5100846.

4 P. Lackner, Z. Zou, S. Mayr, U. Diebold and M. Schmid, Using photoelectron spectroscopy to observe oxygen spillover to zirconia, *Phys. Chem. Chem. Phys.*, 2019, **21**, 17613–17620, DOI: 10.1039/C9CP03322J.

5 H. Li and S. Y. Tong, Forward-focusing and shadowing effects in solids, *Surf. Sci.*, 1993, **281**, L347–L352, DOI: 10.1016/0039-6028(93)90634-V.

6 A. K. Niessen and A. R. Miedema, The enthalpy effect on forming diluted solid solutions of two 4d and 5d transition metals, *Ber. Bunsenges. Phys. Chem.*, 1983, **87**, 717–725, DOI: 10.1002/bbpc.19830870903.

7 Y. Gao, C. Guo, C. Li and Z. Du, Thermodynamic modeling of the Pt–Zr system, *Int. J. Mater. Res.*, 2010, **101**, 819–826, DOI: 10.3139/146.110351.

8 V. Srikrishnan and P. Ficalora, Measurement of the enthalpies of formation of $ZrPt_3$ and $HfPt_3$ by fluorine bomb calorimetry, *Metall. Mater. Trans. B*, 1974, **5**, 1471–1475, DOI: 10.1007/BF02646634.

9 L. Brewer, A most striking confirmation of the Engel metallic correlation, *Acta Metall.*, 1967, **15**, 553–556, DOI: 10.1016/0001-6160(67)90088-0.

10 B. Predel, *Rh-Zr (rhodium-zirconium): Datasheet from Landolt-Börnstein - Group IV · Volume 5J*, DOI: 10.1007/10551312_2631.